Sains Malaysiana 51(5)(2022): 1567-1576
http://doi.org/10.17576/jsm-2022-5105-24

Carrier Density and Thickness Optimization of $In_xGa_{1-x}N$ Layer by Scaps-1D Simulation for High Efficiency III-V Solar Cell

(Pengoptimuman Ketumpatan Pembawa dan Ketebalan Lapisan $In_xGa_{1-x}N$ dengan menggunakan Simulasi Scaps-1D untuk Kecekapan Tinggi Sel Suria III-V)

HABIB ULLAH MANZOOR[1,2], TAN AIK KWAN[1], NG SHA SHIONG[1,*] & ZAINURIAH HASSAN[1]

[1]*Institute of Nano Optoelectronics Research and Technology (INOR), Universiti Sains Malaysia, 11800 USM, Penang, Malaysia*
[2]*University of Engineering and Technology, Lahore-FSD Campus, Pakistan*

Received: 15 July 2021/Accepted: 29 September 2021

ABSTRACT

In this study, the indium gallium nitride ($In_xGa_{1-x}N$) p-n junction solar cells were optimized to achieve the highest conversion efficiency. The $In_xGa_{1-x}N$ p-n junction solar cells with the whole indium mole fraction ($0 \leq x \leq 1$) were simulated using SCAPS-1D software. Optimization of the p- and n-$In_xGa_{1-x}N$ layer's thickness and carrier density were also carried out. The thickness and carrier density of each layer was varied from 0.01 to 1.50 µm and 10^{15} to 10^{20} cm^{-3}. The simulation results showed that the highest conversion efficiency of 23.11% was achieved with x = 0.6. The thickness (carrier density) of the p- and n-layers for this $In_{0.6}Ga_{0.4}N$ p-n junction solar cell are 0.01 (10^{20}) and 1.50 µm (10^{19} cm^{-3}), respectively. Simulation results also showed that the conversion efficiency is more sensitive to the variations of layer's thickness and carrier density of the top p-$In_xGa_{1-x}N$ layer than the bottom n-$In_xGa_{1-x}N$ layer. Besides that, the results also demonstrated that thinner p-$In_xGa_{1-x}N$ layer with higher carrier density offers better conversion efficiency.

Keywords: Photovoltaics; semiconducting indium compounds; solar energy; thin films solar cell; III-V nitride

ABSTRAK

Dalam kajian ini, sel suria indium galium nitrida ($In_xGa_{1-x}N$) bersimpang p-n telah dioptimumkan untuk mencapai kecekapan penukaran yang tertinggi. Sel suria $In_xGa_{1-x}N$ bersimpang p-n dengan keseluruhan pecahan mole indium ($0 \leq x \leq 1$) telah disimulasi dengan menggunakan perisian SCAPS-1D. Pengoptimuman untuk ketebalan dan ketumpatan pembawa bagi lapisan p- dan n-InGaN juga telah dijalankan. Ketebalan dan ketumpatan pembawa bagi setiap lapisan telah diubah daripada 0.01 hingga 1.50 µm dan 10^{15} hingga 10^{20} cm^{-3}. Keputusan simulasi menunjukkan bahawa kecekapan penukaran tertinggi sebanyak 23.11% telah dicapai dengan x = 0.6. Ketebalan (ketumpatan pembawa) bagi lapisan p- dan n- untuk sel suria $In_{0.6}Ga_{0.4}N$ adalah 0.01 (10^{20}) dan 1.50 µm (10^{19} cm^{-3}), masing-masing. Keputusan simulasi juga menunjukkan bahawa kecekapan penukaran adalah lebih sensitif terhadap perubahan ketebalan dan ketumpatan pembawa bagi lapisan p-$In_xGa_{1-x}N$ atas berbanding dengan lapisan n-$In_xGa_{1-x}N$ bawah. Selain itu, keputusan simulasi juga menunjukkan bahawa lapisan p-$In_xGa_{1-x}N$ yang lebih nipis bersama dengan ketumpatan pembawa yang lebih tinggi memberi kecekapan penukaran yang lebih tinggi.

Kata kunci: Fotovolta; sebatian semikonduktor indium; sel suria filem nipis; tenaga suria; III-V nitrida

INTRODUCTION

III-V nitride semiconductors are widely used in the past few decades in optoelectronic devices. Wide direct bandgap indium gallium nitride ($In_xGa_{1-x}N$) ternary alloys are considered pivotal materials in photovoltaic applications because their bandgap energy (E_g) can be engineered to fit the entire solar spectrum (Zhang et al. 2019). Generally, their E_g can be varied from 3.42 (GaN)

to 0.70 eV (InN) by changing indium's mole fraction (Kour et al. 2020). In addition, their intrinsic properties such as high absorption coefficient, high carrier mobility, high drift velocity (Zhang et al. 2019), good saturation velocities (Wang et al. 2018), high thermal stability and conductivity (Kim & Ra 2021), as well as high radiation resistance (Tian et al. 2018), making them an outstanding candidate for high-efficiency solar cell for harsh environments/space applications.

Up to now, many studies have been conducted to improve the conversion efficiency of InxGa1-xN. These include single-junction cells (Akter et al. 2019; Marouf et al. 2018; Moustafa & Alzoubi 2019), PIN junctions (Hussain et al. 2021; Pal & Das 2020), and multi-junctions (Marouf et al. 2019; Rahman et al. 2021). Recently, scientists are developing new techniques to enhance the efficiency of InxGa1-xN p-n junction solar cells (Gupta et al. 2016). For instance, low indium contents InxGa1-xN solar cells were designed (Ayari et al. 2018; Bi et al. 2018; Chouchen et al. 2019; Park et al. 2018). However, this has limited the absorption of the solar cell to shorter wavelengths. Consequently, low indium InxGa1-xN based solar cells with complex structures were developed in order to achieve better conversion efficiency (Belghouthi & Aillerie 2019; Belghouthi et al. 2019; Li et al. 2020; Nath et al. 2020; Shan et al. 2019; Siddharth et al. 2019).

Thickness optimization of the p-n junction $In_xGa_{1-x}N$ solar cell was reported in Feng et al. (2013). The highest conversion efficiency of ~21.5% was obtained at the indium mole fraction of x = 0.6 with the p- and n-$In_xGa_{1-x}N$ layers' thickness of 100 and 4000 nm, respectively. However, optimization of carrier density was not considered. Carrier density is responsible for the number of electrons and holes in a solar cell. Any operation of a solar cell depends upon carrier concentration as it is responsible for charge transportation and electrical current. In order to optimize the performance of a solar cell, the precise value of minority carrier concentration is needed (Uprety et al. 2019) because surface recombination velocity depends upon minority carriers which can affect the conversion efficiency of a solar cell (Smets et al. 2016). Besides that, we also believe that the conversion efficiency of the p-n junction $In_xGa_{1-x}N$ solar cell can further be increased by optimizing the carrier densities of both p- and n-$In_xGa_{1-x}N$ layers.

In this study, $In_xGa_{1-x}N$ p-n junction solar cells with the whole indium mole fraction ($0 \le x \le 1$) were simulated SCAPS-1D software. The thickness and carrier density of the p- and n-$In_xGa_{1-x}N$ layers were optimized to achieve the highest conversion efficiency (η). The obtained results were compared to the simulation results for the simple Si p-n junction solar cell and the reported results for the $In_xGa_{1-x}N$-based solar cells.

Materials and Methods

Model setup and data input

Different $In_xGa_{1-x}N$ p-n junction solar cells were created by varying indium's mole fraction, x and it was varied from 0 to 1.0. Therefore, a total of eleven p-n junction solar cells were simulated. Generally, the mole fraction, $x = 0$ represents GaN ($E_g = 3.42$ eV), and $x = 1.0$ represents InN ($E_g = 0.70$ eV) materials. By changing the indium mole fractions, $In_xGa_{1-x}N$ with different energy bandgaps will be produced. The simulations started with fixed p- and n-$In_xGa_{1-x}N$ layers' thickness and carrier density of 0.50 µm and 10^{17} cm^{-3}. All the $In_xGa_{1-x}N$ parameters used for the simulation were listed in Table 1.

Next, two series of studies were carried out, i.e. (i) optimization of the p- and n-$In_xGa_{1-x}N$ layer's thickness and (ii) optimization of the p- and n-$In_xGa_{1-x}N$ layer's carrier density. The thickness of each layer of the solar cell was optimized by varying it from 0.01 to 1.50 µm. Whereas, the carrier density of each layer was optimized by varying it from 10^{15} to 10^{20} cm^{-3}. It was found in Manzoor et al. (2021) that the optimized thickness of p-InGaN layer was 0.01 µm; hence a minimum thickness of 0.01 µm was considered. A maximum thickness of 1.5 µm was considered because it is still difficult (practically) to grow a very thick and good quality InGaN layer (Liu et al. 2018). All simulations were performed at 300 K using 1.5 AM conditions and irradiance intensity of 1000 W/m^{-2}. Through these simulations, the performance of the solar cell in terms of the open-circuit voltage (V_{oc}), current density (J_{sc}), fill factor (FF), conversion efficiency (), and maximum achieved power density (P_{max}) can be obtained.

Results and Discussion

Optimization of $In_xGa_{1-x}N$ layer's thickness

For this optimization study, the indium mole fraction and the thickness of the p- and n-$In_xGa_{1-x}N$ layers thickness were varied from 0 to 1.0 and 0.10 µm to 1.50 µm, respectively. However, the carrier density of the p- and n-$In_xGa_{1-x}N$ layers was fixed at 10^{17} cm^{-3}. During the optimization, the thickness of one layer was varied at one time while the other was kept fixed at 0.50 µm.

TABLE 1. Simulation parameters for $In_xGa_{1-x}N$ p-n junction solar cells

Parameter	Value / Related equation
Bandgap, E_g (Wu & Walukiewicz 2003)	$x.E_g^{InN} + (1-x).E_g^{GaN} - b.x.(1-x).$ Here x = 0 – 1.0, E_g^{InN} is 0.70 eV and E_g^{GaN} is 3.42 eV. The b is known as the bowing factor, which is equal to 1.43 eV.
Electron affinity, χ (Nawaz & Ahmad 2012)	$4.1 + 0.70(3.42 - E_g)$
Relative permittivity, ε (Zhang et al. 2007)	$15.3x + 8.9(1-x).$
Effective density state of the conduction band N_c (Levinshtein et al. 2001)	$\left(0.9x + 2.3(1-x)\right) \times 10^{18}$ cm^{-3}
Effective density state of the valance band N_v (Levinshtein et al. 2001)	$\left(5.3x + 1.8(1-x)\right) \times 10^{19}$ cm^{-3}
Carrier concentration	1.0×10^{17} cm^{-3}
Capture cross section electrons	1.0×10^{-15} cm^2
Capture cross-section holes	1.0×10^{-15} cm^2
Defect density	1.0×10^{14} cm^{-3}

Figure 1 shows the effects of the p- and n-$In_xGa_{1-x}N$ layers' thickness on the η at different indium mole fractions. Overall, it can be seen that the η is more sensitive to the thickness variation of either p- or n-layer for $In_xGa_{1-x}N$ with indium mode fraction in the range of $0.3 \leq x \leq 0.7$. In this range, it can be noticed from Figure 1(a) that the η of the $In_xGa_{1-x}N$ solar cells reduces with increasing p-$In_xGa_{1-x}N$ thickness. The mole fraction of $0.3 \leq x \leq 0.7$ corresponds to wavelengths of 540 nm to 1020 nm, the region where most of the solar spectrum is, as shown in Figure 2. This spectrum was developed by American Society of Testing Material (ASTM). Typically, as the thickness of the p-$In_xGa_{1-x}N$ layer is increases, the distance between the space charge region and surface increases. As a result, the probability of electron-hole recombination increased and lowered the J_{sc} of the solar cell. Hence, this contributed towards lower η because η = $(J_{sc}V_{oc}FF)/P$ (Wu et al. 2018). In contrast, the η of the

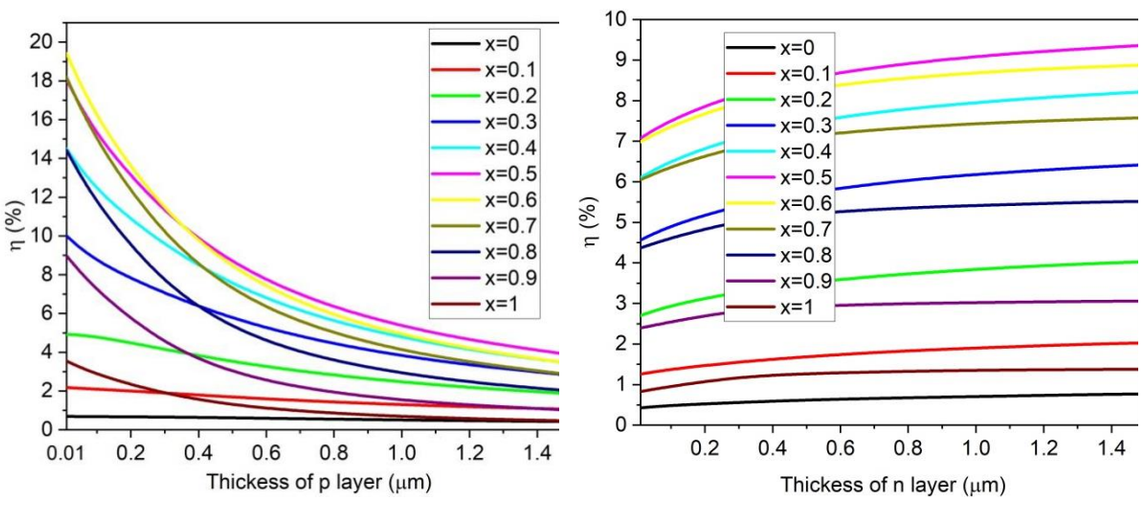

FIGURE 1. Variation of the n as a function of the (a) p- and (b) n-$In_xGa_{1-x}N$ layers thickness. The $In_xGa_{1-x}N$ layer's thickness was varied from 0.01 μm to 1.50 μm

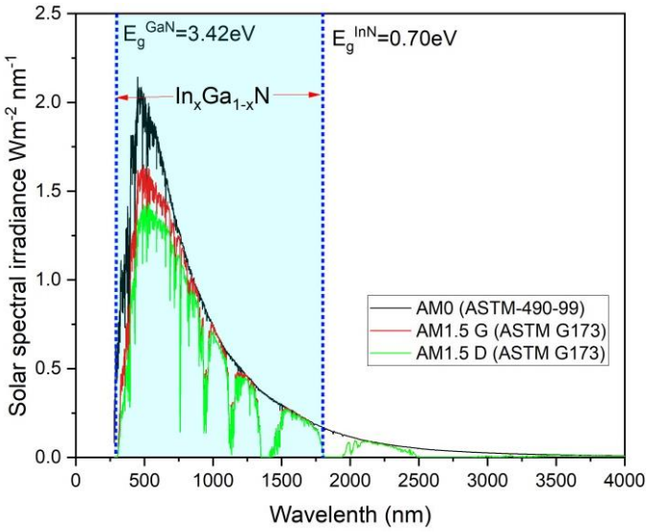

FIGURE 2. Solar spectrum irradiance versus wavelength

$In_xGa_{1-x}N$ solar cells increases slowly with increasing n-$In_xGa_{1-x}N$ thickness, as shown in Figure 1(b). The dependence of η on the n-$In_xGa_{1-x}N$ layer's thickness is insignificant because most of the light is absorbed by the top p-$In_xGa_{1-x}N$ layer (Feng et al. 2013). The results show that the η is more sensitive to the p-$In_xGa_{1-x}N$'s thickness than that of the n-$In_xGa_{1-x}N$.

From Figure 1(a), $In_xGa_{1-x}N$ solar cells with highest η were achieved when the p- and n-$In_xGa_{1-x}N$ thickness is 0.01 µm and 1.50 µm, respectively. These optimization values were selected for the subsequent optimization work on the layer's carrier density. Noted that the η value for the $In_xGa_{1-x}N$ solar cells was gradually increased with increasing the n-$In_xGa_{1-x}N$ thickness; however, a further increase in layer thickness does not contribute significantly towards the η.

OPTIMIZATION OF $IN_XGA_{1-X}N$ LAYER'S CARRIER DENSITY

In this section, the effect of the p- and n-$In_xGa_{1-x}N$ layers' carrier density on the η was investigated by varying carrier density from 10^{15} to 10^{20} cm^{-3}. During the optimization, the carrier density of one layer was varied at one time while the other was kept fixed at 10^{15} cm^{-3}. The effect of the p- and n-$In_xGa_{1-x}N$ layers' carrier density on the η were shown in Figure 3(a) and Figure 3(b), respectively.

From Figure 3(a), it can be seen that the η increases with increasing p-$In_xGa_{1-x}N$ layer's carrier density. Typically, increasing the carrier density in the p-$In_xGa_{1-x}N$ layer will increase the number of holes. Subsequently, this increased the photoconversion and hence the conversion efficiency (η) of the solar cell. Figure 3(a) also shows that the effect of carrier density on the η became more significant for indium mole fraction of $0.4 \leq x \leq 1.0$, where the η increases drastically with the carrier density. According to McAllister et al. (2018) and Zinovchuk and Gryschuk (2018), the Auger coefficient becomes smaller (i.e. the nonradiative recombination losses reduce) at higher carrier density and larger energy bandgap due to the suppression of the Coulomb interactions between free carriers by their mutual shielding. Subsequently, this resulted in higher J_{sc} and hence higher η. Besides that, the electrical field increases and the series resistance reduces as the carrier concentration increases. All these factors contributed to the increase of the η.

As the carrier density increases from 10^{15} cm^{-3} to 10^{20} cm^{-3}, a Burnstein-Moss shift induces a spectral energy shift which widens the energy bandgap (Tessarek et al. 2015). Therefore, the open-circuit voltage increases, V_{oc}. The relation of V_{oc} and carrier density can be explained with equation (1):

$$V_{oc} = \frac{kT}{q} \ln \left[\frac{(N_A + \Delta n)\Delta n}{n_i^2} \right]. \quad (1)$$

where k is the Boltzmann's constant; T is the temperature; q is the charge of an electron; N_A is

the carrier concertation; Δn is the excess carrier concentration; and n_i is the intrinsic concentration. From equation (1), it can be noticed that the V_{oc} increases with increasing carrier concentration. As a result, this contributed towards higher η because $\eta = (J_{sc}V_{oc}FF)/P_{in}$.

Table 2 summarizes the optimized thickness and carrier density of the $In_xGa_{1-x}N$ p-n junction solar cells. It can be seen that the optimized p-$In_xGa_{1-x}N$ layer's carrier density for all the solar cells is 10^{20} cm^{-3}. However, two optimized carrier densities for the n-$In_xGa_{1-x}N$ layer were obtained, i.e., 10^{15} cm^{-3} for solar cells ($0 \leq x \leq 0.4$) and 10^{19} cm^{-3} for solar cells ($0.5 \leq x \leq 1.0$).

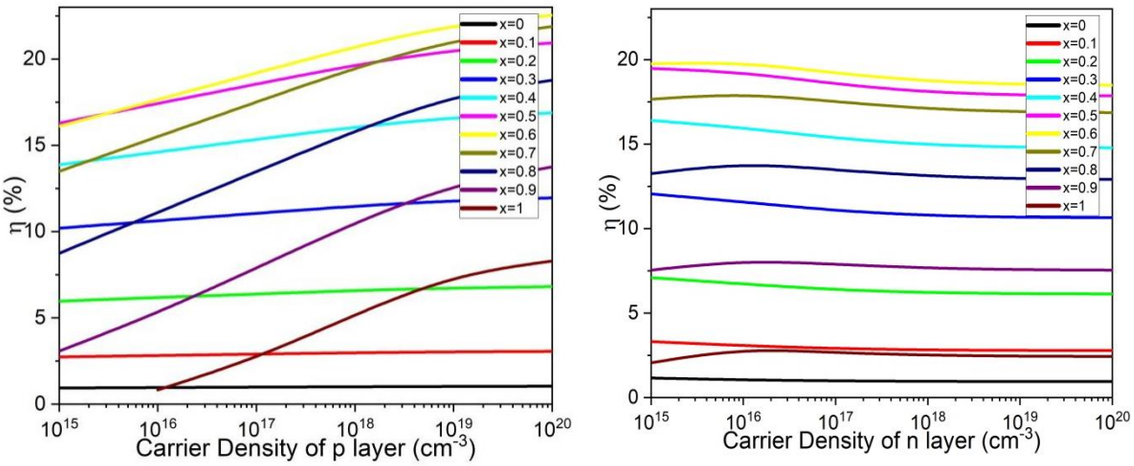

FIGURE 3. Variation of the η as a function of the (a) p- and (b) n- $In_xGa_{1-x}N$ solar cells layer's carrier density as the carrier density varied from 10^{15} to 10^{20} cm^{-3}

TABLE 2. Simulation results of the optimized $In_xGa_{1-x}N$ p-n junction solar cells

Indium Mole fraction, x	Thickness (m)		Carrier density (cm^{-3})		V_{oc} (V)	J_{sc} (mA/cm^2)	FF (%)	η (%)	P_{max} (mW/cm^2)
	p-layer	n-layer	N_a	N_d					
0					2.71	0.50	86.62	1.18	1.18
0.1					2.34	1.64	87.48	3.37	3.37
0.2				10^{15}	1.99	4.11	88.61	7.26	7.26
0.3					1.67	8.39	88.55	12.38	12.38
0.4					1.36	14.11	87.95	16.93	16.93
0.5	0.01	1.50	10^{20}		1.25	18.95	89.43	21.21	21.21
0.6					1.00	26.33	87.52	23.11	23.11
0.7				10^{19}	0.78	34.30	85.18	22.83	22.83
0.8					0.58	39.86	81.77	19.06	19.06
0.9					0.42	45.85	76.92	14.74	14.74
1.0					0.28	52.88	70.50	10.46	10.46

Based on the information gathered in previous sections, $In_xGa_{1-x}N$ p-n junction solar cells for the whole indium mole fraction were simulated, and the results were summarized in Table 2. From Table 2, the highest η of 23.11% was achieved for $In_xGa_{1-x}N$ p-n junction solar cell with $x = 0.6$.

It can be seen from Figure 4, a better quantum efficiency was achieved for a solar cell with mole fractions of $x = 0$ to $x = 0.4$. At these mole fractions, the n-$In_xGa_{1-x}N$ layer of these solar cells has a lower carrier density (i.e. 10^{15} cm^{-3}). Typically, the recombination rate of electrons and holes increases as the carrier density increases, which reduces quantum efficiency, as can be seen for a solar cell with 0.5 x 1.0. It can be seen from Figure 4(b) that as the indium mole fraction increases from 0.1 to 1.0, the wavelength coverage also increases. This can be explained using solar spectrum irradiance, as shown in Figure 2. It can be seen that the InGaN material covers the wavelength from = 360 to = 1800 nm. As indium content increases, so do its covered wavelength region.

Figure 5 represents the variation of the V_{oc}, J_{sc}, η, *FF,* and P_{max} of the p-n junction $In_xGa_{1-x}N$ solar cells as a function of indium's mole fraction. Generally, the V_{oc} is described as the difference in fermi energies of holes and electrons, and it is affected by the energy bandgap. From Figure 5(a), the V_{oc} decreases linearly with decreasing in indium content. However, the J_{sc} increases linearly with increasing in indium content. As the indium's mole content increases, the bandgap of the material will be decreased. Consequently, more photons with longer wavelengths can penetrate deeper into the materials and increase J_{sc}. The η increases from 1.18 to 23.11% when x increases from 0 to 0.6, and the η reduces to 10.46% with further increasing of x. Apart from that, it can be observed from Figure 5(a) and Figure 5(b) that the changes of P_{max} and η with respect to x were similar to each other. In contrast, the *FF* remains almost the same at ~87.00% for $0 \leq x \leq 0.5$, however, further increase in x decreases the *FF* from 88.00% to 70.00%, as shown in Figure 5(b). The *FF* can be measured using equation (2) (Wu et al. 2018), where J_{max} and V_{max} are the current density and voltage at the maximum power point. Here the increase in J_{sc} is more significant than the reduction of V_{oc}, resulting in the reduction of FF.

$$FF = \frac{Jmax \times Vmax}{Jsc \times Voc} \tag{2}$$

As mentioned, Feng et al. (2013) have performed the thickness optimization for the $In_xGa_{1-x}N$ p-n junction solar cells. The highest conversion efficiency of ~21.50% was obtained at $x = 0.6$ with the thickness of 0.10 µm for p-layer and 4.0 µm for n-layer, and both layers have carrier densities of $510^{17}cm^{-3}$. However, by optimizing thickness and carrier density of the $In_xGa_{1-x}N$ p-n junction solar cells, a higher η value of 23.11% was obtained at $x =$ 0.6 with p- and n- $In_xGa_{1-x}N$ layer's thickness and carrier density of 0.01 µm and 1.50 µm, and 10^{20} and 10^{19} cm^{-3}, respectively. The obtained η value of 23.11% is about 7.48% higher than that of Feng et al. (2013). In addition,

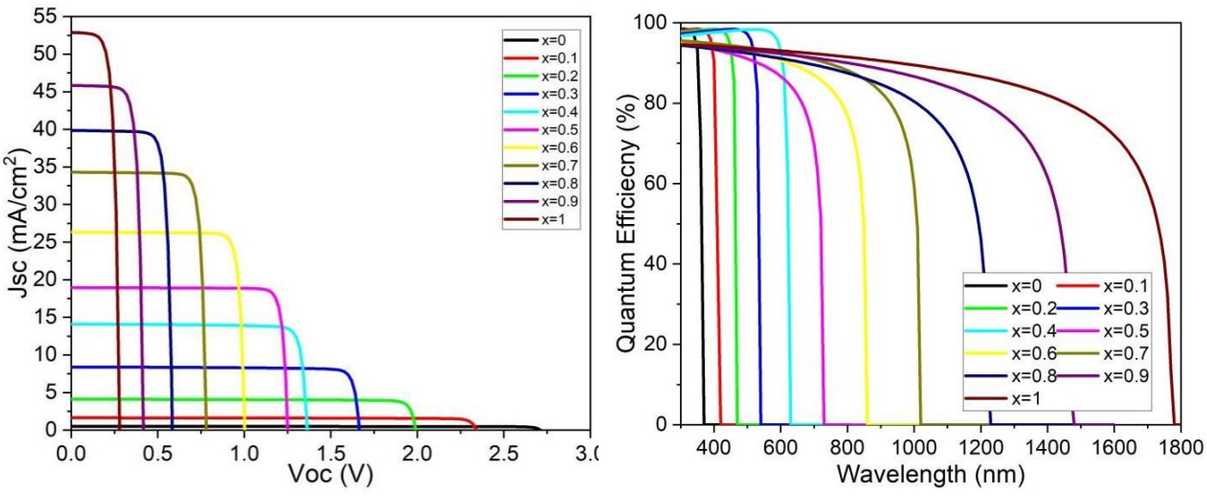

(a) (b)

FIGURE 4. Optimized quantum efficiencies for the $In_xGa_{1-x}N$ p-n junction solar cells

the optimized $In_xGa_{1-x}N$ p-n junction solar cell has thinner p- and n- $In_xGa_{1-x}N$ layer's than that Feng et al. (2013). Basically, this thickness configuration is more practical because the growth rate of the InGaN is very slow, and thick InGaN is hard to achieve. For instance, the growth rate of the InGaN layer with an indium composition of 45% was about 190 nm/h (Yin et al. 2019). Besides that, the dislocation density also increases with increasing InGaN's layer thickness, thus, drastically reducing the quality of the InGaN layer (Kuo & Chang 2016). Therefore, further experimental verification of the present simulation can be performed.

It is known that InN-based semiconductors may replace silicon (Si) semiconductor. For solar cell applications, InGaN-based solar cells provide better conversion efficiency than that of Si. However, no direct comparison on the solar cell structure has been made. In the next section, Si p-n junction solar cells with various p- and n-Si layers thickness (0.01 to 1.50 µm) and carrier density (10^{15} to 10^{20} cm^{-3}) were simulated. The parameters used for simulating the Si p-n junction solar cell were taken from Boumaour et al. (2019). The obtained results were compared to that of the $In_xGa_{1-x}N$ p-n junction solar cells.

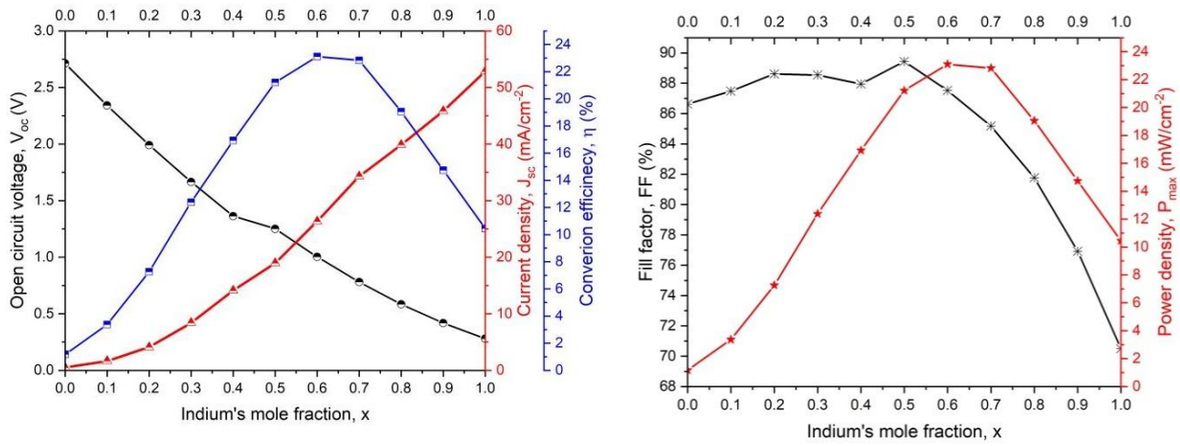

(a) (b)

FIGURE 5. The changes of (a) V_{oc}, J_{sc}, and η, and (b) FF and P_{max} of the $In_xGa_{1-x}N$ p-n junction solar cells as a function of indium mole fraction

Si p-n JUNCTION SOLAR CELL

Figure 6(a) shows the variations of the η as a function of the p- and n-Si layers' thickness. It can be seen that the η is almost constant over the entire range of the p-Si layer's thickness. In contrast, the η keeps on increasing with n-Si layer's thickness. Based on these results, p- and n-Si layers' thickness with the highest η was selected for the simulation with different p- and n-Si layers' carrier densities. Figure 6(b) shows the variations of the η as a function of the p- and n-Si layers' carrier density. Interestingly, it was found that the η exhibits the opposite trends as compared with Figure 6(a), where the η is almost constant over the entire range of the n-Si layer's carrier density and keeps on increasing with p-Si layer's carrier density. The optimization results of Si p-n junction solar was shown in Figure 6(a) and Figure 6(b). The optimized p-layer had a thickness of 0.01 µm and carrier density of 10^{20} cm^{-3}; while the n-layer had a thickness of 1.50 µm and carrier density of 10^{20} cm^{-3}. The optimized p-n junction solar cell provides V_{oc} = 0.61 V, J_{sc} = 10.66 mA/cm^{-2}, FF = 82.63% and η = 5.35%. As compared with the results of $In_{0.6}Ga_{0.6}N$ p-n junction solar cell, it can be seen that using the same configuration, the $In_{0.6}Ga_{0.6}N$ provides 17.67% more η. Furthermore, Si p-n junction solar cell provides η of 12.81% when a thick n-layer of 15.00 µm was used. Generally, surface recombination plays a vital role in the conversion efficiency of any solar cell. However, the surface recombination velocity is limited by minority charge carriers. Therefore, it is beneficial to have a minority charge carrier as low as possible. Typically, the minority charge carriers can be reduced by increasing the doping level of n-type material in silicon p-n junction solar cell. It can also further be

reduced by increasing the thickness of the n-type layer (Smets et al. 2016). Hence, by increasing the n-type doping level to 10^{20} cm^{-3} and its thickness to 15 µm, the conversion efficiency can be increased from 5.35 to 12.81%. From this study, the results implied that a much thicker n-layer is needed to provide higher η in Si p-n junction solar cell while only 1.50 µm thick n-layer is needed in InGaN solar cells.

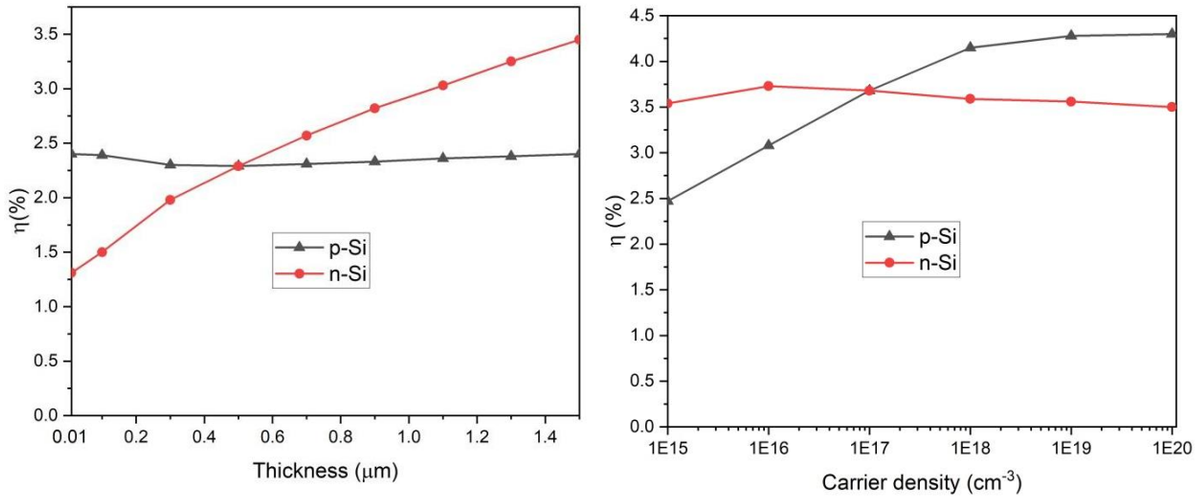

(a) (b)

FIGURE 6. Variation of the η as a function of (a) the p- and n-Si layers' thickness, and (b) the p- and n-Si layers' carrier density

Conclusion

In this study, single p-n junction $In_xGa_{1-x}N$-based solar cells with indium mole fraction (x) varied from 0 to 1.0 were simulated using SCAPS-1D software. The effects of p- and n-$In_xGa_{1-x}N$ solar cells layer's thickness and carrier density on the performance of the solar cells were investigated thoroughly. The results showed that the highest η of 23.11% was obtained for solar cell with x = 0.6, and the thickness (carrier density) of the p- and n-layers is 0.01m (10^{20} cm^{-3}) and 1.50 µm (10^{19} cm^{-3}), respectively. Besides that, the results also showed that the conversion efficiency is more sensitive to the variations of layer's thickness and carrier density of the top p-$In_xGa_{1-x}N$ layer. The results suggested that thinner p-$In_xGa_{1-x}N$ layer with higher carrier density offers better conversion efficiency. The results also showed that the p-n junction $In_xGa_{1-x}N$-based solar cell with the same configurations as the Si solar cell can provide conversion efficiency 4.3 times higher than that of the Si solar cell. This study clearly demonstrated the ability of InGaN semiconductors for the fabrication of high efficiency solar cells.

Acknowledgements

This research was funded by Universiti Sains Malaysia through the Research University Individual (RUI) Grant [Account No.: 1001/CINOR/8011127]. The authors like to thank Mr. Marc Burgelman for his assistance in the development of SCAPS-1D. The first author would like to thank Universiti Sains Malaysia for the sponsored scholarship.

References

Akter, N., Miah, M.S., Matin, M.A. & Amin, N. 2019. Prospect of back contact for a highly efficient ingan thin film solar cell from numerical analysis. In *1st International Conference on Robotics, Electrical and Signal Processing Techniques, ICREST 2019.* ICREST. pp. 622-625.

Ayari, T., Sundaram, S., Li, X., Alam, S., Bishop, C., El Huni, W., Jordan, M.B., Halfaya, Y., Gautier, S., Voss, P.L. & Salvestrini, J.P. 2018. Heterogeneous integration of thin-film InGaN-based solar cells on foreign substrates with enhanced performance. *ACS Photonics* 5(8): 3003-3008.

Belghouthi, R. & Aillerie, M. 2019. Temperature dependence of InGaN/GaN Multiple quantum well solar cells. *Energy Procedia* 157: 793-801.

Belghouthi, R., Aillerie, M., Rached, A. & Mejri, H. 2019. Effect of temperature on electronic and electrical behavior of InGaN double hetero-junction p-i-n solar cells. *Journal of Materials Science: Materials in Electronics* 30(4): 4231-4237.

Bi, Z., Bacon-Brown, D., Du, F., Zhang, J., Xu, S., Li, P., Zhang, J., Zhan, Y. & Hao, Y. 2018. An InGaN/GaN MQWs solar cell improved by a surficial gan nanostructure as light traps. *IEEE Photonics Technology Letters* 30(1): 83-86.

Boumaour, M., Sali, S., Kermadi, S., Zougar, L., Bahfir, A. & Chaieb, Z. 2019. High efficiency silicon solar cells with back ZnTe layer hosting IPV effect: A numerical case study. *Journal of Taibah University for Science* 13(1): 696-703.

Chouchen, B., Gazzah, M.H., Bajahzar, A. & Belmabrouk, H. 2019. Numerical modeling of InGaN/GaN p-i-n solar cells under temperature and hydrostatic pressure effects. *AIP Advances* 9(4): 045313.

Feng, S.W., Lai, C.M., Tsai, C.Y., Su, Y.R. & Tu, L.W. 2013. Modeling of InGaN p-n junction solar cells. *Optical Materials Express* 3(10): 1777.

Gupta, N.D., Janyani, V. & Mathew, M. 2016. Light trapping in p-i-n superlattice based InGaN/GaN Solar cells using photonic crystal. *Optical and Quantum Electronics* 48(11): 1-17.

Hussain, S., Prodhan, M.T. & Rahman, M.M. 2021. Simulation analysis to optimize the performance of homojunction p-i-n In0.7Ga0.3N solar cell. *Semiconductor Physics, Quantum Electronics and Optoelectronics* 24(2): 192-199.

Kim, S.U. & Ra, Y.H. 2021. Modeling and epitaxial growth of homogeneous long-InGaN nanowire structures. *Nanomaterials* 11(1): 9.

Kour, R., Arya, S., Verma, S., Singh, A., Mahajan, P. & Khosla, A. 2020. Review - Recent advances and challenges in Indium Gallium nitride (In x Ga 1-x N) materials for solid state lighting. *ECS Journal of Solid State Science and Technology* 9(1): 015011.

Kuo, Y.K. & Chang, J.Y. 2016. Effect of composition-graded interlayers in double-heterostructure blue InGaN light-emitting diodes. *Physica Status Solidi (A) Applications and Materials Science* 213(1): 154-157.

Levinshtein, M.E., Rumyantsev, S.L. & Shur, M.S. 2001. *Properties of Advanced Semiconductor Materials: GaN, AIN, InN, BN, SiC, SiGe*. New Jersey: John Wiley & Sons. pp. 1-216.

Li, X.Y., Shan, H.S. & Zheng, J. 2020. Statistical analysis of the photoelectric characteristics for InGaN/GaN MQWs solar cells following proton irradiation. *ECS Journal of Solid State Science and Technology* 9(5): 055014.

Liu, J., Liang, H., Xia, X., Abbas, Q., Liu, Y., Luo, Y., Zhang, Y., Yan, L., Han, X. & Du, G. 2018. Anomalous Indium incorporation and optical properties of high Indium content InGaN grown by MOCVD. *Journal of Alloys and Compounds* 735: 1239-1244.

Manzoor, H.U., Zawawi, M.M., Pakhuruddin, M.Z., Ng, S.S. & Hassan, Z. 2021. High conversion and quantum efficiency Indium-rich p-InGaN/p-InGaN/n-InGaN solar cell. *Physica B: Condensed Matter* 622: 413339.

Marouf, Y., Dehimi, L., Bouzid, F., Pezzimenti, F. & Della Corte, F.G. 2018. Theoretical design and performance of InxGa1-XN single junction solar cell. *Optik* 163: 22-32.

Marouf, Y., Dehimi, L. & Pezzimenti, F. 2019. Simulation study for the current matching optimization in In0.48Ga0.52N/In0.74Ga0.26N dual junction solar cells. *Superlattices and Microstructures* 130: 377-389.

McAllister, A., Bayerl, D. & Kioupakis, E. 2018. Radiative and auger recombination processes in Indium Nitride. *Applied Physics Letters* 112(25): 1-6.

Moustafa, M.O. & Alzoubi, T. 2019. Numerical simulation of single junction ingan solar cell by scaps. In *Key Engineering Materials*, edited by Korsunsky, A.M. Bäch SZ: Trans Tech Publications Ltd. pp. 407-413.

Nath, P., Biswas, A. & Nath, V. 2020. Performance optimization of solar cells using non-polar, semi-polar and polar InGaN/GaN multiple quantum wells alongside AlGaN blocking layers. *Microsystem Technologies* 27(1): 301-306.

Nawaz, M. & Ahmad, A. 2012. A TCAD-based modeling of GaN/InGaN/Si solar cells. *Semiconductor Science and Technology* 27(3): 035019.

Pal, D. & Das, S. 2020. Numerical simulation of GaN/InGaN p-i-n solar cells: Role of interlayers in promoting photovoltaic response. *Optik* 221: 165403.

Park, J.H., Nandi, R., Sim, J.K., Um, D.Y., Kang, S., Kim, J.S. & Lee, C.R. 2018. A III-nitride nanowire solar cell fabricated using a hybrid coaxial and uniaxial InGaN/GaN multi quantum well nanostructure. *RSC Advances* 8(37): 20585-20592.

Rahman, M.A., Islam, M.J., Islam, M.R. & Mahmud, M.P. 2021. Strain dependent performance analysis of InGaN multi-junction solar cell. *Transactions on Electrical and Electronic Materials* 22: 833-842.

Shan, H.S., Li, X.Y., Chen, B., Ma, S.F., Li, L. & Xu, B.S. 2019. Effect of indium composition on the microstructural properties and performance of InGaN/GaN MQWs solar cells. *IEEE Access* 7: 182573-182579.

Siddharth, G., Garg, V., Sengar, B.S., Bhardwaj, R., Kumar, P. & Mukherjee, S. 2019. Analytical study of performance parameters of InGaN/GaN multiple quantum well solar cell. *IEEE Transactions on Electron Devices* 66(8): 3399-3404.

Smets, A.H., Jäger, K., Isabella, O., Swaaij, R.A. & Zeman, M. 2015. *Solar Energy: The Physics and Engineering of Photovoltaic Conversion, Technologies and Systems*. Cambridge: UIT Cambridge. pp. 1-484.

Tessarek, C., Goldhahn, R., Sarau, G., Heilmann, M. & Christiansen, S. 2015. Carrier-induced refractive index change observed by a whispering gallery mode shift in GaN microrods. *New Journal of Physics* 17(8): 83047.

Tian, M., Qian, Y.D., Zhang, C., Li, L., Yao, S.D., Ferguson, I.T., Talwar, D.N., Zhai, J.Y., Meng, D.H., He, K.Y. & Wan, L.Y. 2018. Investigation of high Indium-composition InGaN/GaN heterostructures on ZnO grown by metallic organic chemical vapor deposition. *Optical Materials Express* 8(10): 3184.

Uprety, P., Subedi, I., Junda, M.M., Collins, R.W. & Podraza, N.J. 2019. Photogenerated carrier transport properties in silicon photovoltaics. *Scientific Reports* 9(1): 1-12.

Wang, T., Wang, X., Chen, Z., Sun, X., Wang, P., Zheng, X., Rong, X., Yang, L., Guo, W., Wang, D. & Cheng, J. 2018. High-mobility two-dimensional electron gas at InGaN/InN heterointerface grown by molecular beam epitaxy. *Advanced Science* 5(9): 1-7.

Wu, S., Cheng, L. & Wang, Q. 2018. Effects of the unintentional background concentration, Indium composition and defect density on the performance of InGaN p-i-n homojunction solar cells. *Superlattices and Microstructures* 119: 9-18.

Wu, J., Walukiewicz, W., Yu, K.M., Shan, W., Ager Iii, J.W., Haller, E.E., Lu, H., Schaff, W.J., Metzger, W.K. & Kurtz, S. 2003. Superior radiation resistance of In 1-XGa XN alloys: Full-solar-spectrum photovoltaic material system. *Journal of Applied Physics* 94(10): 6477-6482.

Yin, H., Qian, Y., Xie, L., Song, C., Wang, X., Chen, H., Wang, P., Zhou, G. & Nötzel, R. 2019. Electrocatalytic activity of InN/InGaN quantum dots. *Electrochemistry Communications* 106: 106514.

Zhang, X., Wang, X., Xiao, H., Yang, C., Ran, J., Wang, C., Hou, Q. & Li, J. 2007. Simulation of In0.65Ga0.35 N single-junction solar cell. *Journal of Physics D: Applied Physics* 40(23): 7335-7338.

Zhang, Y., Guo, R., Xu, S., Zhang, J., Zhao, S., Wang, H., Hu, Q., Zhang, C. & Hao, Y. 2019. High-performance high electron mobility transistors with GaN/InGaN composite channel and superlattice back barrier. *Applied Physics Letters* 115(7): 072105.

Zinovchuk, A.V. & Gryschuk, A.M. 2018. Alloy-assisted auger recombination in InGaN. *Optical and Quantum Electronics* 50(12): 1-8.

*Corresponding author; email: shashiong@yahoo.com